analytical chemistry

Article

pubs.acs.org/ac

Plasmonic Nanorice Antenna on Triangle Nanoarray for Surface-Enhanced Raman Scattering Detection of Hepatitis B Virus DNA

Ming Li,[†] Scott K. Cushing,[†,‡] Hongyan Liang,[§] Savan Suri,[†] Dongling Ma,[§] and Nianqiang Wu*[,†]

[†]Department of Mechanical and Aerospace Engineering and [‡]Department of Physics, West Virginia University, Morgantown, West Virginia 26506-6106, United States

[§]Institut National de la Recherche Scientifique, INRS-Énergie, Matériaux et Télécommunications, 1650 Boulevard Lionel-Boulet, Varennes, Québec J3X 1S2, Canada

Supporting Information

ABSTRACT: The sensitivity and the limit of detection of Raman sensors are limited by the extremely small scattering cross section of Raman labels. Silver nanorice antennae are coupled with a patterned gold triangle nanoarray chip to create spatially broadened plasmonic "hot spots", which enables a large density of Raman labels to experience strong local electromagnetic field. Finite difference time domain simulations have confirmed that the quasi-periodic structure increases the intensity and the area of the surface plasmon resonance (SPR), which enhances the surface-enhanced Raman scattering (SERS) signal significantly. The SERS signal of the nanorice/DNA/nanoarray chip is compared with that of the nanorice/DNA/film chip. The SERS signal is greatly enhanced when the Ag nanorices are coupled to the periodic Au nanoarray instead of the planar film chip. The resulting spatially broadened SPR field enables the SERS biosensor with a limit of detection of 50 aM toward hepatitis B virus DNA with the capability of discriminating a single-base mutant of DNA. This sensing platform can be extended to detect other chemical species and biomolecules such as proteins and small molecules.

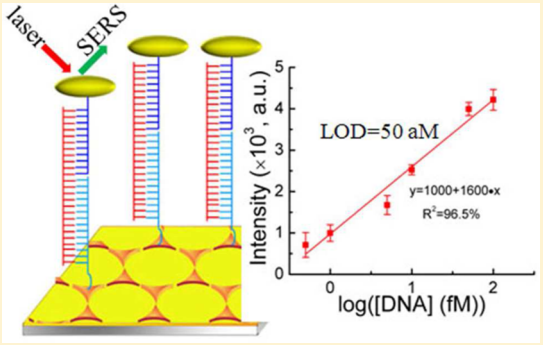

Surface-enhanced Raman scattering (SERS) offers multiplexed detection with a single excitation wavelength in commercially available, portable Raman microscopes. It is a potential technique for point-of-care applications in biological and chemical sensing.[1−5] Sensors based on Raman labels have advantages over those based on fluorescent labels.[6−10] In fluorescent assays, organic dyes suffer from photobleaching while inorganic quantum dots are vulnerable to fluorescence quenching by the complex sample matrix. Raman sensors overcome both shortcomings. However, Raman scattering is extremely inefficient due to the small Raman scattering cross section of molecules ($\sim 10^{-30}$ to 10^{-25} cm^2), which is significantly smaller than the fluorescence cross section ($\sim 10^{-16}$ cm^2).[11]

The SERS intensity of Raman labels can be amplified via two mechanisms, that is, chemical enhancement (CE) and electromagnetic (EM) enhancement. The EM enhancement originates from localized surface plasmon resonance (LSPR) that concentrates the incident light, creating intense local EM fields.[6,12−18] Since the SERS signal is proportional to the fourth power of the EM field, the limit of detection (LOD) of SERS sensors can be greatly increased by optimizing the size, shape, and composition of plasmonic nanostructures.[19−24] Currently, nanoparticles suspended in a solution are widely used as the SERS detection platforms,[25−29] in which the SERS signal is enhanced by covalently anchoring Raman labels onto the plasmonic gold (or silver) nanoparticle surface. The SERS signal can be further enhanced by the formation of small, high intensity "hot spots" when two nanoparticles are brought into close proximity so that their LSPR fields are coupled. Various nanoparticle geometries have been explored to optimize the intensity of the hot spots in a solution or on a metallic film.[25−29] Despite these attempts, the LOD of nanoparticle-based SERS sensors has been restricted to the picomolar level.[30,31] To further improve the LOD of SERS sensors, it is desired to increase the coupled plasmonic field both in intensity and in space.

The most promising route to increase the spatial extent of the LSPR field is pairing colloids with periodic nanostructures. LSPR in periodic and aperiodic plasmonic nanostructures can lead to EM enhancement over a large volume because of coupling between repeated components of the array.[32−37] A periodic nanostructure can be applied to a sensor by coupling nanoparticles with a planar periodic array via DNA hybridization. When the DNA hybridization takes place, the resulting plasmonic field will increase both in space and in intensity due to the quasi-periodicity of the overall pattern. The spatially broadened EM field will enhance the SERS signal of Raman

Received: July 27, 2012
Accepted: January 15, 2013
Published: January 15, 2013

reporters, further lowering the LOD. The signal-to-noise ratio in coupled plasmonic sensors is determined by the difference in the LSPR enhancement before and after hybridization.

Herein, a SERS sensor is constructed based on the Ag nanorice@Raman label@SiO_2 sandwich nanoparticles that are coupled to a periodic Au triangle nanoarray via the linkage of hepatitis B virus (HBV) DNA. Such architecture is expected to result in the spatially enhanced EM field of the quasi-perioidic array, leading to ultrasensitive SERS detection. In the sandwich nanoparticles, malachite green isothiocyanate (MGITC) molecules are chosen as the Raman labels that are embedded between the Ag nanorice core and the SiO_2 shell. The plasmonic Ag nanorice acts as the SERS substrate. The thin SiO_2 shell renders the water solubility and provides a platform for conjugation of molecular recognition elements.[6,7] This sandwich nanostructure also concentrates the Raman labels and prevents them from leaching during the sensing process.[6,7] The designed SERS sensor is used for detection of HBV DNA, since hepatitis B is a prevalent and potentially life-threatening disease caused by the HBV. Chronic carriers of "inactive" HBV often have no symptoms but can still transmit the virus to others. Hepatitis B can lead to chronic liver disease, cirrhosis of the liver, and even liver cancer. About 350 million people worldwide are chronic carriers of HBV, and more than 620 000 die from liver-related diseases each year.[38] In the United States alone, about 800 000 to 1.4 million people are chronic HBV carriers, many of whom are undiagnosed. HBV causes around 3000 deaths each year.[38] It is imperative to develop a highly sensitive and inexpensive sensor as a point-of-care device for early detection of HBV.

EXPERIMENTAL SECTION

Chemicals and Materials. Malachite green isothiocyanate (MGITC) was purchased from Molecular Probes, Inc. 3-Triethoxylsilylpropyl succinic anhydride (TEPSA) was purchased from Gelest Inc. (3-Aminopropyl) trimethoxylsilane (APTMS), 5 M NaCl solution, sodium silicate stock solution (26.5% SiO_2 in 10.6% Na_2O), *N*-hydroxysuccinimide (NHS), 1-ethyl-3-(3-dimethylaminopropyl)-carbodiimide (EDC), 11-mercaptoundecanoic acid (MUA), and 11-mercapto-1-undecanol (MU) were purchased from Sigma–Aldrich. Na_2HPO_4 (99.0%) and NaH_2PO_4 (99.0%) came from Alfa Aesar. HBV DNAs used in the work were obtained from Integrated DNA Technologies (IDT), and the sequences are listed in Table 1.[39]

Table 1. Sequences of Single-Stranded DNAs Used in Present Work

name	sequence
DNA-capture probe	3′-NH_2-C_6-TAT GGT GTA GTA GGT-5′
DNA-detection probe	5′-NH_2-C_6-TGG CTT TCA GTT ATA-3′
DNA target	5′-ATA CCA CAT CCA TAT AAC TGA AAG CCA-3′
single-base mismatched DNA	5′-ATA CCA CAT CCA CAT AAC TGA AAG CCA-3′

Deionized (D.I.) water was produced by a Milli-Q Millipore system (18.2 MΩ·cm, Millipore Corp). All solvents were obtained from the commercial sources and used without further purification.

Synthesis of Sandwich Nanoparticles. Ag nanorice was synthesized by a polyol process reported previously.[40] Ag nanorice@MGITC@SiO_2 sandwich nanoparticles were prepared according to a procedure described below. First, 1 mL of the as-synthesized Ag nanorice solution (optical density, OD = 2.73; concentration = ~10^{10} mL^{-1}) was centrifuged and washed with ethanol at least 5 times to remove the surfactants on the Ag nanorice surface, and then, it was redispersed into 8 mL of ethanol. Fresh APTMS aqueous solution (100 μL, 2.0 mM) was added and stirred for 30 min to coat the Ag nanorice surface with the amine group. MGITC aqueous solution (500 μL, 100 μM) was dropwise added with constant stirring for an additional 30 min. Following this, 50 μL of fresh sodium silicate (0.54 wt %) was added and stirred for 10 min, followed by addition of 4 mL of ethanol. This suspension was kept undisturbed for one day before an additional 4 mL of ethanol was added and then kept another day to generate a thin and dense SiO_2 layer. Finally, the resulting suspension was centrifuged and washed with ethanol to remove some impurities, and the precipitates were collected.

Fabrication of Au Triangle Nanoarray Chip. The Au triangle nanoarray on a Si wafer was fabricated using the nanosphere lithography technique.[41,42] Briefly, a monolayer of hexagonally close packed polystyrene spheres (500 nm in a diameter) were self-assembled on a Si wafer. A 10 nm thick titanium and a 50 nm thick Au layer were then deposited on the Si wafer using e-beam evaporation. Subsequently, the chips were sonicated in ethanol to lift off the polystyrene spheres, leaving an array of Au triangles on the Si wafer.

DNA Functionalization of Sandwich Nanoparticles and Au Chip. The Ag nanorice@MGITC@SiO_2 sandwich nanoparticles obtained above were redispersed into ethanol to obtain an ethanolic solution (OD ≈ 2.7). TEPSA (100 μL) was added to 100 μL of sandwich nanoparticle suspension and then incubated for 4 h to achieve carboxyl group-terminated sandwich nanoparticles. After centrifugation, 100 μL of phosphate-buffered saline (PBS) solution containing 50 mM NHS and 200 mM EDC was added and incubated for 2 h to activate the carboxyl group for DNA conjugation by carbodiimide chemistry.[6,7] In the next step, 50 μL of 20 μM signaling probe was added and incubated overnight. The resulting suspension was centrifuged and washed with a cleaning buffer (10 mM Na_2HPO_4/NaH_2PO_4, 0.3 M NaCl, and pH = 7.0) to remove excessive DNA. As a result, the DNA–sandwich nanoparticle conjugates were achieved and then dispersed into a hybridization buffer solution (100 mM Na_2HPO_4/NaH_2PO_4, 0.75 M NaCl, and pH = 7.0) for future use. The loading of attached DNA was around 63 signaling probes per sandwich nanoparticle based on the intensity of absorption peak in the UV–visible spectrum (1 OD_{260} = 7 nmol/L shown in IDT's report).

Functionalization of the chips (Au triangle nanoarray and the Au planar film) was carried out according to our previous paper.[7] Briefly, the chips were cleaned by plasma etching and successive immersion in CH_2Cl_2, D.I. water, and ethanol each for 10 min and then dried in a vacuum oven at 60 °C for 1 h. The cleaned chips were incubated overnight in an ethanolic solution containing 100 mM MUA and 100 mM MU and then washed with ethanol and D.I. water, respectively. The resulting MUA/MU-modified chips were activated by immersion in a PBS solution containing 50 mM NHS and 200 mM EDC for 2 h. The activated MUA/MU-modified chips were immersed in a PBS solution of 20 μM DNA-capture probe. After immobilization of the DNA-capture probe, the chips were successively rinsed with the cleaning buffer solution to remove excessive DNA.

dx.doi.org/10.1021/ac303387a | *Anal. Chem.* 2013, 85, 2072–2078

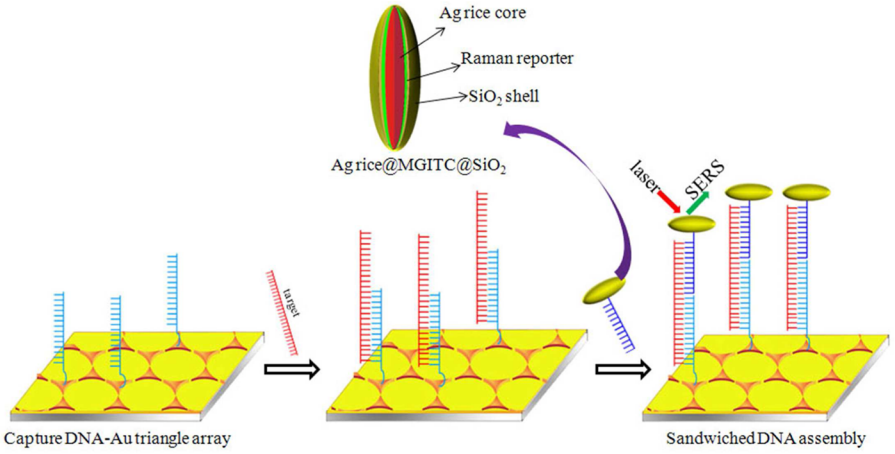

Figure 1. Schematic illustration of the sandwich structure of Ag nanorice@Raman label@SiO_2 and the operating principle of the SERS sensor for HBV DNA detection. Zoom-in: the sandwich structure of Ag nanorice@Raman label@SiO_2.

Characterization. UV−visible absorption spectra were acquired by a Shimadzu UV-2550 spectrometer. Scanning electron microscopy (SEM) and transmission electron microscopy (TEM) images were collected with a field-emission JEOL JSM-7600F scanning electron microscope and a JEOL JEM-2100F transmission electron microscope, respectively, at an acceleration voltage of 200 kV. Fourier transform infrared (FT-IR) spectra were obtained from the chips under the attenuated total reflection (ATR) mode with a Thermo Nicolet 6700 spectrometer.

DNA Detection. Figure S1 of the Supporting Information shows the schematic configuration of a portable Raman spectrometer (Inspector Series, DeltaNu), which is suitable for point-of-care detection in remote environments. Raman spectra were recorded in the range from 200 to 2200 nm under excitation of a 785 nm laser. Calibration and normalization of the Raman spectra were done with polystyrene. Three spectra from different sites were collected from each sample and averaged to represent the SERS results. The maximum laser power on the sample was around 0.011 mW, which was measured by a power meter (Newport, model-1918-R). The SERS acquisition time was 10 s.

Finite Difference Time Domain Simulations. Following our previous work,[6,43] finite difference time domain (FDTD) simulations were performed using the open source MEEP (an acronym for MIT Electromagnetic Equation Propagation) code. An explanation of the implementation of the FDTD algorithm and perfectly matched layer (PML) layers in MEEP can be found in the ref 44. The dielectric function used for both Ag and Au was a series of four Lorentz sums fitted to the data of Johnson and Christy.[45] The fitting for Au and Ag was first optimized to match the values predicted by Mie theory for a 15 nm nanosphere.[46] It was also checked if theoretical absorption curves for the Ag nanorice matched the experimental data. The simulated Ag nanorices were 400 nm in length and 60 nm in a diameter. The absorption of the nanorice matched the experimental data. The data of the dimensions of the Au triangle array were taken from the SEM image. A mesh size of 1 nm was used in all simulations, and convergence was checked up to this mesh size. To output the three-dimensional (3D) EM field, a plane wave, constant wavelength source at 785 nm was utilized, and the boundary conditions were perfectly matched layers. The EM field was output over several times throughout the entire volume and normalized against the input source power. The incident wave vector was always perpendicular to the surface. Both parallel and perpendicular polarizations were tested for all the shapes in order to replicate experimental conditions. The polarization corresponding to the largest EM field enhancement is shown in the EM field visualizations. A background dielectric constant of 1.33 was used to replicate the liquid phase of the sensor. The visualization was done in the open source MayaVI2 software.

RESULTS AND DISCUSSION

Operating Principle of SERS Sensor. A sandwich architecture of nanoparticle/analyte/chip was used in the SERS sensor (Figure 1). The nanoparticle also has a sandwich structure of Ag nanorice@MGITC@SiO_2, as shown in Figure 1. On average, the Ag nanorice core had a diameter of 50 nm and a length of 300 nm (Figure 2a), and the SiO_2 shell was 5−6 nm thick (Figure 2b). The Ag nanorice showed two strong

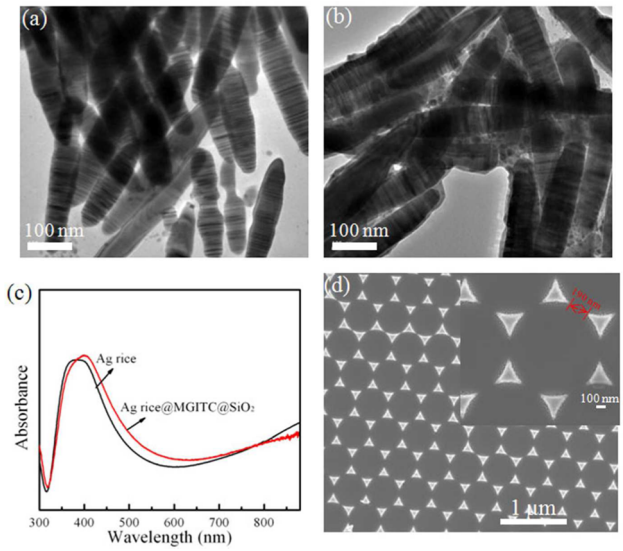

Figure 2. TEM images of (a) Ag nanorice and (b) Ag nanorice@MGITC@SiO_2 sandwich nanoparticles; (c) UV−visible absorption spectra of Ag nanorice and Ag nanorice@MGITC@SiO_2 sandwich nanoparticles; (d) SEM image of the Au triangle nanoarray pattern on the Si substrate. Inset: the zoom-in SEM image of the Au triangle nanoarray.

dx.doi.org/10.1021/ac303387a | Anal. Chem. 2013, 85, 2072−2078

LSPR bands at 400 and 1500 nm, respectively (Figure S2, Supporting Information). A less than 15 nm redshift of the LSPR band was observed after the Ag nanorice was coated with a SiO_2 shell (Figure 2c). The nonfluorescent Raman reporter (MGITC) was covalently bound onto the Ag nanorice core. The sandwich nanoparticles showed the characteristic Raman spectrum of MGITC (Figure S3, Supporting Information). The assignments of SERS peaks of MGITC are listed in Table S1 of the Supporting Information. The DNA-detection probe was conjugated on the surface of the Ag nanorice@MGITC@SiO_2 nanoparticle (Figure S4a, Supporting Information). The chip used was a Au triangle nanoarray pattern on the Si wafer (Figure S4b, Supporting Information), which was fabricated with nanosphere lithography.[41,42] The Au triangle pattern was fabricated with 500 nm polystyrene spheres, and the closest gap between two adjacent triangle dots was 190 nm (Figure 2d). This Au triangle nanoarray acted as the periodic plasmonic substrate. The DNA-capture probe was immobilized on the surface of Au triangles on the chip (Figure 1). FT-IR measurement has confirmed the successful immobilization of DNA-capture probe on the chip (Figure S5, Supporting Information).

The DNA detection process included two hybridization steps that were performed in a humid chamber (Figure 1). The chip functionalized with the DNA-capture probe was first immersed in a solution containing the DNA target. After 10 min of incubation, the chip was rinsed by the buffer solution to remove excessive DNA. Subsequently, the chip was immersed in a buffer solution containing the sandwich nanoparticles conjugated with the DNA-detection probe. After 0.5 h of incubation, the nanoparticle/DNA/chip structure was formed. After a vigorous washing with the cleaning buffer solution, the Raman spectrum of MGITC was collected from the nanoparticle/DNA/chip structure. The Raman intensity was dependent on the number of the sandwich nanoparticles coupled to the chip, which was directly proportional to the concentration of the DNA target.

Detection of DNA with SERS Sensor. The above-mentioned SERS sensor was used to detect the HBV DNA. Figure 3a shows the SERS spectra that corresponded to various concentrations of the HBV DNA target (0.01 fM to 2.0 nM). A negligible SERS signal was detected when the concentration of the DNA target was below 0.05 fM. The SERS intensity increased significantly with an increase in the concentration of the DNA target. The SERS intensity became saturated when the DNA concentrations exceeded 1.0 pM. Figure 3c depicts the calibration curve that plotted the intensity of the SERS peak at 1335 cm^{-1} as the logarithmic concentration of the DNA target. The calibration curve in Figure 3d showed a linear range from 0.5 to 100 fM. In the linear region, the least-squares fitting was $y = 1000 + 1600x$ with a regression coefficient (R^2) of 96.5%, where y is the SERS intensity at 1335 cm^{-1} and x is the logarithmic concentration of the DNA target. According to the International Union of Pure and Applied Chemistry (IUPAC) standard, the LOD was estimated to be 50 aM based on the $3s/m$ criterion,[47] where m is the slope for the linear range and s is the standard deviation of the blank ($n = 10$; n is the number of spectra acquired). Table 2 lists the performance data of different DNA measurement techniques such as fluorescence, polymerase chain reaction (PCR), electrochemistry, and colorimetry.[48−56] It can be seen that the LOD of the SERS sensor in the present work was significantly lower than those of most sensors based on conventional methods. The LOD is

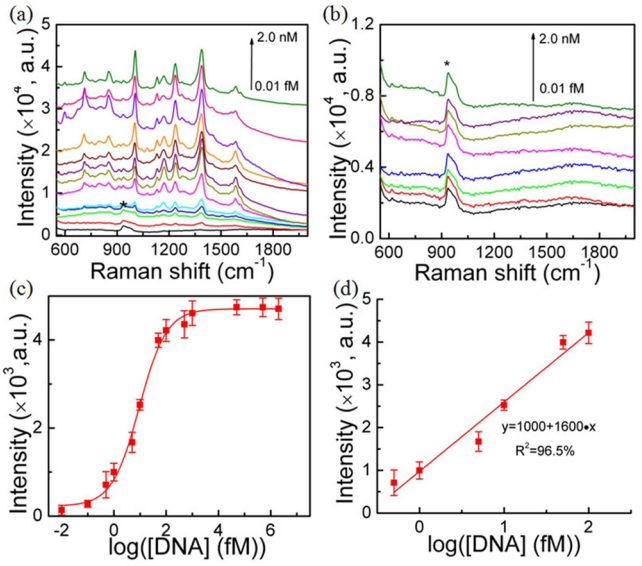

Figure 3. SERS spectra taken from the nanoparticle/target/triangle nanoarray with various concentrations of DNA of (a) HBV DNA target (0.01 fM, 0.1 fM, 0.5 fM, 1.0 fM, 5.0 fM, 10 fM, 50 fM, 0.1 pM, 0.5 pM, 1.0 pM, 50 pM, 0.5 nM, and 2.0 nM) and (b) single-base mismatched DNA (0.01 fM, 0.1 fM, 0.5 fM, 1.0 fM, 10 fM, 0.1 pM, 1.0 pM, and 2.0 nM); (c) plot of the Raman intensity at 1335 cm^{-1} as a function of the logarithmic concentration of HBV DNA and (d) the linear region of (c).

governed by several factors, including (i) the signal amplification capability of the local plasmonic field of SERS substrate, (ii) the affinity of the DNA target with the capture and detection probes, which is dependent on the dissociation constant, (iii) the noise level of instrumentation, and other factors. The present work is focused on the development of a new nanoarchitecture that is able to generate a strong plasmonic field.

The selectivity of the nanoparticle/analyte/chip sensor was tested with the single-base mutants of HBV DNA. Figure 3b shows the SERS spectra in the presence of various concentrations of single-base mutants. No SERS peak of MGITC was observed even when the concentration of the single-base mutant increased as high as 2.0 nM. This indicated that the DNA hybridization cannot happen in the case of single-base mismatched mutants, which confirmed extremely high selectivity of this DNA sensor.

SERS Enhancement by Plasmonic Nanostructures. The SERS sensor based on the nanoparticle/analyte/chip architecture showed a very low LOD toward HBV DNA. The major reason was that the SERS signal of MGITC was significantly amplified by the EM enhancement of the plasmonic nanoparticle/DNA/chip nanostructure. FDTD simulations were performed to clarify this point. Figure 4a shows the 3D EM field distribution surrounding the free-standing Ag nanorice. It was seen that the Ag nanorice had a local EM field enhancement $|E|^2$ of ∼50 (Figure 4a), which created a SERS enhancement $|E|^4$ of ∼2,500. A similar simulation result was seen for the Au triangle nanoarray (Figure 4b). The largest local EM field enhancement $|E|^2$ was ∼14, which created a SERS enhancement $|E|^4$ of ∼200. Simulation was performed with the incident EM field polarizations along the short and long axis of both geometries; only the strongest EM field enhancement is shown in Figure 4.

dx.doi.org/10.1021/ac303387a | Anal. Chem. 2013, 85, 2072−2078

Table 2. Summary of the Performance Data of DNA Sensors Reported Previously

sensing system	sensing principle	type of assay	linear range (M)	LOD (M)	ref
DNA/Au microarray	SPR imaging	direct	not determined (ND)	1.0×10^{-8}	48
Au nanoparticle/DNA/Au film	SPR reflectance	direct	ND	$\sim 1.0 \times 10^{-14}$	49
SiO_2 nanoparticle/DNA/glass	fluorescence	sandwich	ND	8.0×10^{-16}	50
ND	PCR	direct	2.88 to 2.69 $\times 10^{7}$ IU/mL	56 IU/mL	51
dye/DNA/quantum dot	fluorescence	sandwich	0 to 5.0×10^{-7}	4.0×10^{-9}	39
methylene blue/DNA/electrode	electrochemistry	sandwich	ND	1.0×10^{-13}	52
Au nanoparticle/DNA/Au electrode	conductance	sandwich	ND	5.0×10^{-13}	53
molecular beacon/exonuclease III	colorimetry	sandwich	2.0×10^{-17} to 2.0×10^{-13}	1.0×10^{-14}	54
Pb−Sn/DNA/Al substrate	scanning calorimetry	sandwich	ND	8.0×10^{-14}	55
Au nanoparticles	colorimetry	direct	ND	1.0×10^{-12}	56
our SERS sensor	SERS	sandwich	5.0×10^{-16} to 1.0×10^{-13}	50 aM	

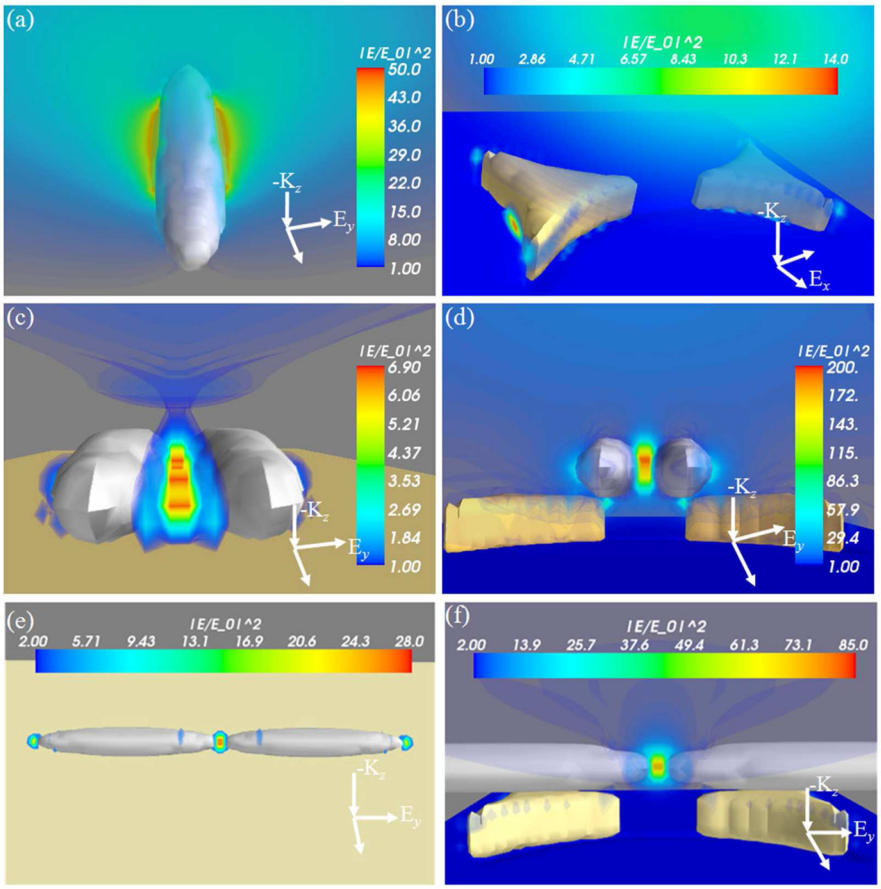

Figure 4. 3D FDTD simulated electromagnetic field enhancement of (a) Ag nanorice, (b) Au triangle nanoarray, (c, e) Ag nanorices coupled to the planar Au film, and (d, f) Ag nanorices coupled to the Au triangle nanoarray. The electromagnetic field enhancement scale is normalized by $|E/E_0|^2$, and the applied incident laser wavelength is 785 nm, perpendicular to the surface. K_z refers to the incident wavevector, and E_x or E_y refers to the electric field polarization for the simulation.

It should be noted that the EM field enhancements of both the Ag nanorice and the Au triangle array are not optimized for the Raman laser wavelength.

When the Ag nanorice and the Au triangle array were coupled into proximity (Figure 4d,f), the intensity of the local EM field increased not only in its magnitude but also significantly in its spatial distribution. The exact distribution of the Ag nanorice on top of the Au triangle array cannot be simulated. To replicate experimental conditions, several base arrangements of Ag nanorice on the Au triangle nanoarray were tested, of which superpositions could be made to create any orientation. It was seen that, when the nanorice formed dimers on top of the Au triangle array (Figure 4d,f), the signal was orders of magnitude higher than that in plane orientations (Figure S6, Supporting Information). The nanorice will attach to the triangular array in a random orientation. In this random orientation, several dimers of all orientations are expected to exist. Even if few dimers assemble in permutations close to the optimal position, the signal produced by these pairs will be orders of magnitude higher than the other orientations, dominating the SERS signal. Therefore, the peak sensor response can be approximated by the nanorice orientations that lead to the highest EM field response.

dx.doi.org/10.1021/ac303387a | *Anal. Chem.* 2013, 85, 2072−2078

In an optimized position with the nanorice forming dimers on the top of the triangle, the normalized local EM field due to LSPR showed an enhancement $|E|^2$ of ~85 or ~200 depending on orientation, which theoretically resulted in a SERS enhancement $|E|^4$ of ~7000 and ~40 000. This is at least an order of magnitude increase in signal as compared to the other sensor configurations. In particular, the coupling mode between the triangular array and short axis of the nanorice creates a spatially broadened plasmonic field of high intensity. The low LOD in the coupled plasmonic SERS sensor can be associated with the formation of spatially broadened plasmonic hot spots in the randomly oriented coupled colloidal nanorice/triangle substrate array during DNA hybridization. The resulting SERS signal is much higher in the presence of the analyte than the uncoupled structures, leading to an increased LOD.

To demonstrate that the spatially broadened plasmonic hot spot was a result of the quasi-periodic array and not the formation of randomly oriented Ag nanorice dimers, the simulations were repeated with the Au triangle nanoarray substituted by a Au planar film. The FDTD simulations show the opposite situation when the Ag nanorice are coupled to the Au planar film (Figure 4c,e). Figure 4c,e shows the EM field for the same nanorice/film configuration. The LSPR-induced local EM field distribution increased spatially for coupling but was weakened in the peak intensity. This negative effect was due to the fact that the dielectric constant of the Au film shifted the longitudinal LSPR of the Ag nanorice further from the excitation wavelength (785 nm) used in the SERS sensor. In addition, the gold planar film can dampen the resonance, since image charges were created in the Au conductor, leading to a loss in the EM field intensity. Previous reports have shown small high-intensity hot spots between a nanoparticle and film. However, no such spots existed under the excitation of the 785 nm laser.

To confirm the FDTD simulation results of the nanorice/film and the nanorice/nanoarray structures, the SERS signals of the nanoparticle/analyte/nanoarray chip and the nanoparticle/analyte/film chip were measured in the presence of 1.0 pM HBV DNA (Figure 5). The SERS spectrum of the nanoparticle/analyte/nanoarray chip in the presence of single-base mismatch DNA is also shown for comparison. It can be observed that the nanoparticle/DNA/nanoarray chip exhibited a significantly stronger SERS signal than the nanoparticle/DNA/film chip in the case of identical HBV DNA concentrations. These results have demonstrated that a lower LOD is possible for an existing DNA-based colloidal detection scheme simply by switching to a quasi-periodic coupled plasmonic nanoarchitecture.

The lower LOD is a result of the ~10^4 EM field enhancement distributed over a large area and the large difference between the background signal of the uncoupled nanorice and the signal of the coupled pattern. Although previously reported plasmonic architectures have shown hot spots with EM field enhancements as high as 10^6–10^8, the enhancement is focused on a hot spot in a few nanometers and is not always conditional in the presence of the analyte. The spatially broadened hot spot enhances the SERS even when few Raman reporters are present, leading to a low LOD. The advantage of a periodic architecture is that it creates a distributed enhancement of the EM field, which even at lower EM field, enhancement factors can still greatly reduce the LOD as demonstrated in the detection of HBV DNA.

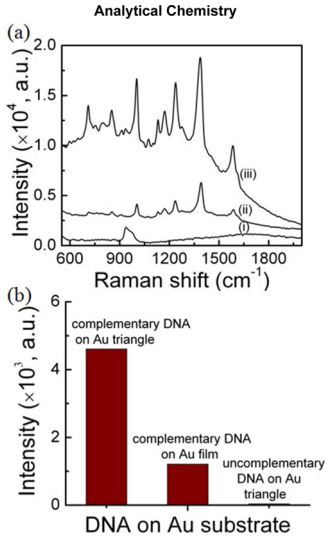

Figure 5. (a) SERS spectra of (i) single-base mismatched DNA on the Au triangle nanoarray, (ii) complementary DNA on the Au film, and (iii) complementary DNA on the Au triangle nanoarray; (b) the SERS intensity at 1335 cm^{-1} in the presence of the 1.0 pM complementary DNA or the single-base mismatched DNA in the nanoparticle/DNA/nanoarray chip and the nanoparticle/DNA/film chip.

CONCLUSIONS

In summary, a SERS sensor was developed for ultrasensitive detection of HBV DNA. The SERS signal was detected when the Ag nanorice@MGITC@SiO_2 sandwich nanoparticles were coupled to a Au triangle nanoarray via the linkage of the DNA target. The coupling between the sandwich nanoparticles and the Au triangle nanoarray created an intense, spatially distributed electromagnetic field. As a result, the SERS sensor was able to sensitively detect the HBV DNA with a limit of detection as low as 50 aM. The SERS sensor can effectively discriminate and detect a single-base mismatch mutant of HBV DNA. By comparing the SERS intensities of the nanoparticle/DNA/nanoarray chip and the nanoparticle/DNA/film chip, it has been concluded that the spatially increased plasmonic field in coupled quasi-periodic arrays can improve the LOD of the SERS sensor. The sensor engineered in this report can be extended to detection of other analytes such as small molecules, proteins, viruses, and explosives.

ASSOCIATED CONTENT

Supporting Information

Additional information as noted in the text. This material is available free of charge via the Internet at http://pubs.acs.org.

AUTHOR INFORMATION

Corresponding Author

*Fax: +1-304-293-6689; e-mail: nick.wu@mail.wvu.edu.

Notes

The authors declare no competing financial interest.

ACKNOWLEDGMENTS

The resource and facilities used were partially supported by NSF (EPS 1003907) and a Research Challenge Grant from the State of West Virginia (EPS08-01), the West Virginia University Research Corporation, and the West Virginia EPSCoR Office. The use of WVU shared facility was acknowledged. S.K.C. is supported by the National Science

Foundation Graduate Research Fellowship under grant no. 1102689. D.M. is grateful to the financial support from the Natural Sciences and Engineering Research Council of Canada and Fonds de la recherche sur la nature et les technologies.

REFERENCES

(1) Graham, D. *Angew. Chem., Int. Ed.* **2010**, *49*, 9325−9327.
(2) Barhoumi, A.; Halas, N. J. *J. Am. Chem. Soc.* **2010**, *132*, 12792−12793.
(3) Oh, Y.-J.; Park, S.-G.; Kang, M.-H.; Choi, J.-H.; Nam, Y.; Jeong, K.-H. *Small* **2011**, *7*, 184−188.
(4) Qian, X.; Peng, X.-H.; Ansari, D. O.; Yin-Goen, Q.; Chen, G. Z.; Shin, D. M.; Yang, L.; Young, A. N.; Wang, M. D.; Nie, S. *Nat. Biotechnol.* **2008**, *26*, 83−90.
(5) Ma, S.; Livingstone, R.; Zhao, B.; Lombardi, J. R. *J. Phys. Chem. Lett.* **2011**, *2*, 671−674.
(6) Li, M.; Cushing, S. K.; Zhang, J.; Lankford, J.; Aguilar, Z. P.; Ma, D.; Wu, N. *Nanotechnology* **2012**, *23*, 115501.
(7) Li, M.; Zhang, J.; Suri, S.; Sooter, L. J.; Ma, D.; Wu, N. *Anal. Chem.* **2012**, *84*, 2837−2842.
(8) Li, M.; Li, R.; Li, C. M.; Wu, N. Q. *Front. Biosci., Scholar Ed.* **2011**, *3*, 1308−1331.
(9) Zhang, H.; Harpster, M. H.; Wilson, W. C.; Johnson, P. A. *Langmuir* **2012**, *28*, 4030−4037.
(10) Golightly, R. S.; Doering, W. E.; Natan, M. J. *ACS Nano* **2009**, *3*, 2859−2869.
(11) Kneipp, K.; Moskovits, M.; Kneipp, H. *Top. Appl. Phys.* **2006**, *103*, 261−278.
(12) Kneipp, K.; Kneipp, H.; Itzkan, I.; Dasari, R. R.; Feld, M. S. *Chem. Rev.* **1999**, *99*, 2957−2975.
(13) Jackson, J. B.; Halas, N. J. *Proc. Natl. Acad. Sci. U.S.A.* **2004**, *1*, 17930−17935.
(14) Hong, J. W.; Lee, S.-U.; Lee, Y. W.; Han, S. W. *J. Am. Chem. Soc.* **2012**, *134*, 4565−4568.
(15) Haynes, C. L.; Van Duyne, R. P. *J. Phys. Chem. B* **2003**, *107*, 7426−7433.
(16) Dadosh, T.; Sperling, J.; Bryant, G. W.; Breslow, R.; Shegai, T.; Dyshel, M.; Haran, G.; Bar-Joseph, I. *ACS Nano* **2009**, *3*, 1988−1994.
(17) McFarland, A. D.; Young, M. A.; Dieringer, J. A.; Van Duyne, R. P. *J. Phys. Chem. B* **2005**, *109*, 11279−11285.
(18) Alvarez-Puebla, R.; Liz-Marzán, L. M.; de Abajo, F. J. G. *J. Phys. Chem. Lett.* **2010**, *1*, 2428−2434.
(19) Álvarez-Puebla, R. A. *J. Phys. Chem. Lett.* **2012**, *3*, 857−866.
(20) Jensen, T. R.; Malinsky, M. D.; Haynes, C. L.; Van Duyne, R. P. *J. Phys. Chem. B* **2000**, *104*, 10549−10556.
(21) Lee, K.-S.; El-Sayed, M. A. *J. Phys. Chem. B* **2005**, *109*, 20331−20338.
(22) Liz-Marzán, L. M. *Langmuir* **2006**, *22*, 32−41.
(23) Zhang, Q.; Li, N.; Goebl, J.; Lu, Z.; Yin, Y. *J. Am. Chem. Soc.* **2011**, *133*, 18931−18939.
(24) Zhang, J.; Li, S.; Wu, J.; Schatz, G. C.; Mirkin, C. A. *Angew. Chem., Int. Ed.* **2009**, *48*, 7787−7791.
(25) Barman, I.; Dingari, N. C.; Kang, J. W.; Horowitz, G. L.; Dasari, R. R.; Feld, M. S. *Anal. Chem.* **2012**, *84*, 2474−2482.
(26) Feng, Y.; Wang, Y.; Wang, H.; Chen, T.; Tay, Y. Y.; Yao, L.; Yan, Q.; Li, S.; Chen, H. *Small* **2012**, *8*, 246−251.
(27) Brown, L. O.; Doorn, S. K. *Langmuir* **2008**, *24*, 2277−2280.
(28) Kim, N. H.; Lee, S. J.; Moskovits, M. *Nano Lett.* **2010**, *10*, 4181−4185.
(29) Ochsenkühn, M. A.; Jess, P. R. T.; Stoquert, H.; Dholakia, K.; Campbell, C. J. *ACS Nano* **2009**, *3*, 3613−3621.
(30) Tsoutsi, D.; Montenegro, J. M.; Dommershausen, F.; Koert, U.; Liz-Marzán, L. M.; Parak, W. J.; Alvarez-Puebla, R. A. *ACS Nano* **2011**, *5*, 7539−7546.
(31) Dasary, S. S. R.; Singh, A. K.; Senapati, D.; Yu, H.; Ray, P. C. *J. Am. Chem. Soc.* **2009**, *131*, 13806−13812.
(32) Li, W.-D.; Ding, F.; Hu, J.; Chou, S. Y. *Opt. Express* **2011**, *19*, 3925−3936.
(33) Xu, J.; Zhang, L.; Gong, H.; Homola, J.; Yu, Q. *Small* **2011**, *7*, 371−376.
(34) Xu, J.; Kvasnička, P.; Idso, M.; Jordan, R. W.; Gong, H.; Homola, J.; Yu, Q. *Opt. Express* **2011**, *19*, 20493−20505.
(35) Caldwell, J. D.; Glembocki, O.; Bezares, F. J.; Bassim, N. D.; Rendell, R. W.; Feygelson, M.; Ukaegbu, M.; Kasica, R.; Shirey, L.; Hosten, C. *ACS Nano* **2011**, *5*, 4046−4055.
(36) Zhang, X.-Y.; Hu, A.; Zhang, T.; Lei, W.; Xue, X.-J.; Zhou, Y.; Duley, W. W. *ACS Nano* **2011**, *5*, 9082−9092.
(37) Cho, W. J.; Kim, Y.; Kim, J. K. *ACS Nano* **2012**, *6*, 249−255.
(38) Department of Communicable Disease Surveillance and Response. *Hepatitis B*; World Health Organization: Geneva, Switzerland, 2002.
(39) Wang, X.; Lou, X.; Wang, Y.; Guo, Q.; Fang, Z.; Zhong, X.; Mao, H.; Jin, Q.; Wu, L.; Zhao, H.; Zhao, J. *Biosens. Bioelectron.* **2010**, *25*, 1934−1940.
(40) Liang, H.; Zhao, H.; Rossouw, D.; Wang, W.; Xu, H.; Botton, G. A.; Ma, D. *Chem. Mater.* **2012**, *24*, 2339−2346.
(41) Li, H.; Low, J.; Brown, K. S.; Wu, N. Q. *IEEE Sens. J.* **2008**, *8*, 880−884.
(42) Li, H.; Wu, N. Q. *Nanotechnology* **2008**, *19*, 275301.
(43) Cushing, S. K.; Hornak, L. A.; Lankford, J.; Liu, Y.; Wu, N. Q. *Appl. Phys. A: Mater. Sci. Process.* **2011**, *103*, 955−958.
(44) Oskooi, A. F.; Roundy, D.; Ibanescu, M.; Bermel, P.; Joannopoulos, J. D.; Johnson, S. G. *Comput. Phys. Commun.* **2010**, *181*, 687−702.
(45) Johnson, P. B.; Christy, R. W. *Phys. Rev. B* **1972**, *6*, 4370−4379.
(46) Mayer, K. M.; Hafner, J. H. *Chem. Rev.* **2011**, *111*, 3828−3857.
(47) Gilfrich, J. V.; Birks, L. S. *Anal. Chem.* **1984**, *56*, 77−79.
(48) Nelson, B. P.; Grimsrud, T. E.; Liles, M. R.; Goodman, R. M.; Corn, R. M. *Anal. Chem.* **2001**, *73*, 1−7.
(49) He, L.; Musick, M. D.; Nicewarner, S. R.; Salinas, F. G.; Benkovic, S. J.; Natan, M. J.; Keating, C. D. *J. Am. Chem. Soc.* **2000**, *122*, 9071−9077.
(50) Zhao, X.; Tapec-Dytioco, R.; Tan, W. *J. Am. Chem. Soc.* **2003**, *125*, 11474−11475.
(51) Welzel, T. M.; Miley, W. J.; Parks, T. L.; Goedert, J. J.; Whitby, D.; Ortiz-Conde, B. A. *J. Clin. Microbiol.* **2006**, *44*, 3325−3333.
(52) Xia, F.; White, R. J.; Zuo, X.; Patterson, A.; Xiao, Y.; Kang, D.; Gong, X.; Plaxco, K. W.; Heeger, A. J. *J. Am. Chem. Soc.* **2010**, *132*, 14346−14348.
(53) Park, S.-J.; T. Taton, A.; Mirkin, C. A. *Science* **2002**, *295*, 1503−1506.
(54) Zuo, X.; Xia, F.; Xiao, Y.; Plaxco, K. W. *J. Am. Chem. Soc.* **2010**, *132*, 1816−1818.
(55) Wang, C.; Ma, L.; Chen, L.-M.; Chai, K. X.; Su, M. *Anal. Chem.* **2010**, *82*, 1838−1843.
(56) Xu, W.; Xie, X.; Li, D.; Yang, Z.; Li, T.; Liu, X. *Small* **2012**, *8*, 1846−1850.